Influence of Geometrical Constraints on Propagation in Cardiac Tissue

S Jacquir[1], S Binczak[1], G Laurent[2], P Athias[2], JM Bilbault[1]

[1]Laboratoire LE2I UMR CNRS 5158, Université de Bourgogne, Dijon, France
[2]Institut de Recherche Cardiovasculaire, CHU Le Bocage, Dijon, France

Abstract

The behaviour of impulse propagation in the presence of non-excitable scar and boundaries is a complex phenomenon and induces pathological consequences in cardiac tissue. In this article, a geometrical configuration is considered so that cardiac waves propagate through a thin strand, which is connected to a large mass of cells. At this interface, waves can slow down or even be blocked depending on the width of the strand. We present an analytical approach leading to determine the blockage condition, by introducing planar travelling wavefront and circular stationary wave. Eventually, the influence of the tissue geometry is examined on the impulse propagation velocity.

1. Introduction

Reentry is the major mechanism of life-threatening ventricular arrhythmias associated with myocardial infarction scar [1]. In abnormal conditions, electrical cardiac wavefront may be stopped by, for instance, electrically non-excitable scar or functional block, which may induce a reentry circuit in pathological endocardial tissue. Nevertheless, normal geometrical features may also imply variations of the conduction properties, as accessory atrioventricular pathways, consisting of narrow strands of myocyte coursing from atrium to ventricle [2]. Therefore, the architecture of the cellular network forming the myocardium [3, 4] and the geometry of excitation wavefront [5, 6, 7] are important to characterize the impulse propagation. Mathematical models [8, 9] and nonlinear dynamics are widely used to study the impulse (action potential) propagation in cardiac cells [10, 11, 12]. Among them, one of the major model is described by the FitzHugh-Nagumo (FHN) equation [13], which allows analytical approaches. The goal of this paper is to study the propagation condition in a system composed of a thin strand of myocytes connected to a large mass of cells. This geometry is modelled using a modified version of the FHN equation. We show that, at the interface of the two parts of the system, the shape of the waves goes through a geometrical modification, which can lead to a decrease of the velocity up to a blockage phenomenon. Eventually, we determine the optimal width of the strand which minimizes the time delay at the interface.

2. Methods and results

We consider a thin sheet of myocardium such as a two-dimensional model is used to describe the impulse propagation. The medium is assumed to be isotropic and its schematic design is sketched in Fig. 1. In the bounded do-

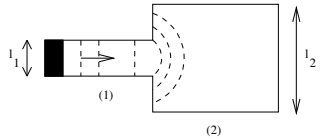

Figure 1. Schematic diagram of the geometry of the tissue. l_1 (resp. l_2) is the width of the domain (1) (resp. domain (2)). Arrow indicates direction of propagation.

main, the corresponding equations modelling this system are:

$$\begin{cases} \dfrac{\partial V}{\partial t} = D\Delta V - f(V) - W \\ \dfrac{\partial W}{\partial t} = \varepsilon(V - \gamma W)\ , \end{cases} \tag{1}$$

where D is the diffusion parameter, t is the time, Δ is the continuous Laplacian operator, V is the transmembrane voltage. W is the recovery variable, which indicates the capacity of the medium to revert to its resting state after the propagation of impulsions, due to potassium current and the nonlinear function $f(V)$ represents the behaviour of the sodium current. Usually, $f(V)$ is a cubic polynomial function, but a common simplification is to approximate this function by a piecewise linear expression. Furthermore, characterizing the velocity of the action potential corresponds to determine the velocity of the leading edge of this wave, which is given by the condition $W(t) = 0\ \forall t$. The system (1) becomes

$$\frac{\partial V}{\partial t} = D\Delta V - [V - H(V - \alpha)], \tag{2}$$

where α is a threshold between the passive and the active role of the sodium conductance ($0 < \alpha < 1/2$) and H is the Heaviside step function. This system is completed by the Neumann boundary conditions, so that

$$\frac{\partial V}{\partial n} = 0 \,, \tag{3}$$

where $\frac{\partial}{\partial n}$ denotes the outer normal derivative at the boundary of the bounded domain. To investigate a propagation at the interface, we initiate a wavefront in domain (1). Due to the width of the strand, we assume this wave to be planar and propagating towards domain (2). The symmetry induced by this choice of configuration allows us to reduce the system to continuous one-dimensional medium so that it can be described by the following bistable equation,

$$\frac{\partial V}{\partial t} = D\frac{\partial^2 V}{\partial x^2} - [V - H(V-\alpha)] \,. \tag{4}$$

Introducing the travelling frame coordinate $\xi = x - ct$, where c is the front velocity, eq. (4) can be written so that

$$D\frac{\partial^2 V}{\partial \xi^2} + c\frac{\partial V}{\partial \xi} - [V - H(V-\alpha)] = 0 \,, \tag{5}$$

which yields, due to C^0 continuity, the propagating solution in domain (1):

$$\begin{cases} V(\xi) = \alpha e^{\lambda_{2,1}\xi}, & \text{if } V < \alpha \\ V(\xi) = (\alpha - 1)e^{\lambda_{1,2}\xi} + 1, & \text{if } V \geq \alpha \,, \end{cases} \tag{6}$$

where $\lambda_{1,2} = -\frac{c}{2D} \pm \frac{1}{2}\sqrt{(\frac{c}{D})^2 + \frac{4}{D}}$.
Note that in [14], the stability of this kind of solution in an infinite medium has been analyzed. Note also that this solution has been observed and confirmed by numerical simulations.
When this wave reaches the interface, a symmetry breaking occurs, depending on the width l_1 (resp. l_2) of the domain (1) (resp. domain (2)):
- if $l_1 \leq l_c \ll l_2$, the incoming wave is pinned at the interface, where l_c is a critical width to be determined,
- if $l_2 > l_1 > l_c$, the wave is transformed in either circular (l_1 small) or elliptic one (l_1 large),
- if $l_1 = l_2$, we observe a planar propagation in domain (2), according to (6).

In the blockage situation, numerical simulations show that the shape of the standing wave is circular. Therefore, it corresponds to the existence of a circular standing solution in domain (2).
In order to determine the critical value l_c, we need to express the standing solution in the case of a circular wave. Because of this circular symmetry, we look for a time independent solution $V(r)$ with r radial coordinate, leading to express eq. (2), so that

$$D(\frac{\partial^2 V}{\partial r^2} + \frac{1}{r}\frac{\partial V}{\partial r}) = V - H(V-\alpha). \tag{7}$$

Introducing $\rho = r\sqrt{\frac{1}{D}}$ eq. (7) becomes

$$(\frac{\partial^2 V}{\partial \rho^2} + \frac{1}{\rho}\frac{\partial V}{\partial \rho}) = V - H(V-\alpha) \,. \tag{8}$$

Let r_a be defined so that $V(r_a) = \alpha$.

- if $V < \alpha$, eq. (8) becomes $\frac{\partial^2 V}{\partial \rho^2} + \frac{1}{\rho}\frac{\partial V}{\partial \rho} - V = 0$ and the standing solution is

$$V(\rho) = A_1 I_0(\rho) + B_1 K_0(\rho) \,, \tag{9}$$

where I_0 and K_0 represent the modified Bessel functions of the first and second kind respectively.
- if $V \geq \alpha$, eq. (8) becomes $\frac{\partial^2 V}{\partial \rho^2} + \frac{1}{\rho}\frac{\partial V}{\partial \rho} - V + 1 = 0$ and the standing solution is

$$V(\rho) = 1 + A_2 I_0(\rho) + B_2 K_0(\rho). \tag{10}$$

We impose the following conditions leading to find the constants A_1, B_1, A_2 and B_2:

- $V(r \to \infty) = 0$ leading to $A_1 = 0$.
- $V(r = 0) = V_0 > \alpha$ leading to $B_2 = 0$. V_0 is the maximal amplitude of an initial condition corresponding to $r = 0$.

Eventually, due to C^0 continuity, the standing wave solution is

$$\begin{cases} V(r) = \dfrac{\alpha K_0(\frac{r}{\sqrt{D}})}{K_0(\frac{r_a}{\sqrt{D}})}, & \text{if } r \geq r_a \\ \\ V(r) = 1 + (\alpha - 1)\dfrac{I_0(\frac{r}{\sqrt{D}})}{I_0(\frac{r_a}{\sqrt{D}})}, & \text{if } r < r_a \,, \end{cases} \tag{11}$$

where r_a is determined by:

$$r_a = \sqrt{D} I_0^{-1}(\frac{\alpha - 1}{V_0 - 1}). \tag{12}$$

An illustration of such a wave is presented in Fig. 2.

The standing solution given by eq. (11) allows the determination of the critical width l_c. Indeed, the blockage situation corresponds to the case where an incoming planar propagating wave in domain (1) gives birth to the circular standing wave in domain (2). Like the Huygens principle in optical scattering, each elementary cell is assumed to give rise to a circular wave, which leads in a first approximation to a global circular propagating wave flowing in domain (2). Recognizing that initiation of a travelling wave in domain (2) requires a minimum area where the

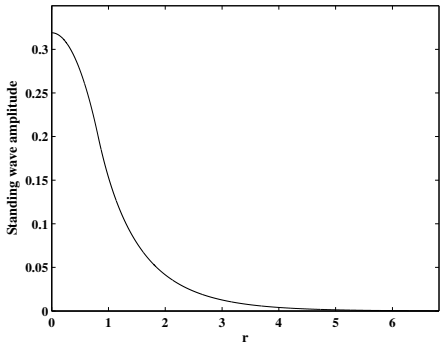

Figure 2. Cross-section of the standing wave with $D = 1$, $\alpha = 0.2$, $r_a = 0.8186$ and $V_0 = 0.319$.

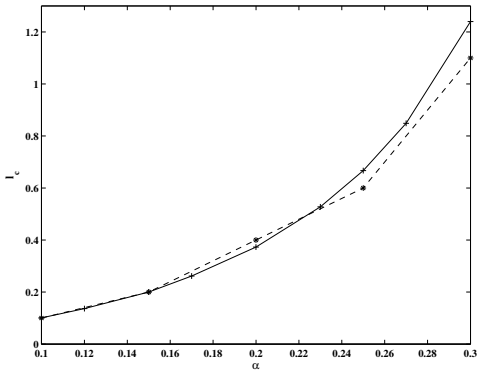

Figure 3. l_c versus α ($D = 1$). Theoretical results (cf eq.(14)) in continuous line, numerical results in dashed line.

cells are excited (*i.e.* $V > \alpha$), we assume that this area, in the case of blockage is the location of the transformed planar wave with a null velocity and where $V > \alpha$. As $c = 0$, it implies

$$V(r) = (\alpha - 1)e^{\sqrt{\frac{1}{2D}}(r - r_c)} + 1 \,, \qquad (13)$$

where $r_c = l_c/2 = r_a$. When $r \geq r_a$ ($V \leq \alpha$) the spatial distribution corresponds to the previously defined circular standing wave (first equation of system (11)). The C^0 and C^1 conditions of continuity lead to determine l_c from r_c implicitly obtained by

$$(\alpha - 1)\sqrt{\frac{1}{2D}} + \frac{\alpha K_1(r_c\sqrt{\frac{1}{D}})}{K_0(r_c\sqrt{\frac{1}{D}})} = 0. \qquad (14)$$

A comparison between this theoretical prediction and numerical simulations shows a good match between them as illustrated in Fig. 3 (based on a finite difference scheme using a 4^{th} order Runge-Kutta on a $100 * 100$ mesh).
Besides the numerical confirmation of the blockage phenomenon when $l_1 \leq l_c$, numerical simulations indicate that the emergence of propagating wave in domain (2) induces a time delay due to the transformation of the planar travelling wave to a non-zero curvature wavefront. Actually, this delay is required so that cells reach the threshold excitation, as observed experimentally [2]. In this section, we present a numerical study showing the relationship between velocity, intrinsic parameters of the model and geometrical features. The basic morphological features of the transition region between a domain (1) and a domain (2) are depicted on Fig 4, where l is the width of the do-

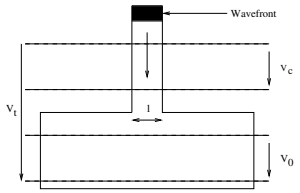

Figure 4. Schematic diagram of the geometry of the tissue.

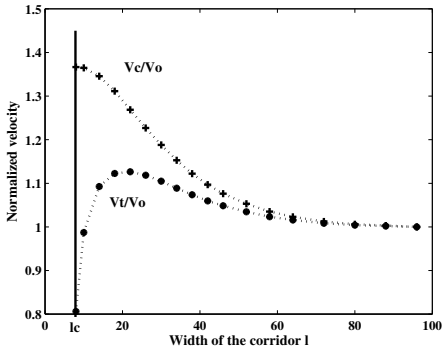

Figure 5. Wavefront velocity versus the width of the corridor.

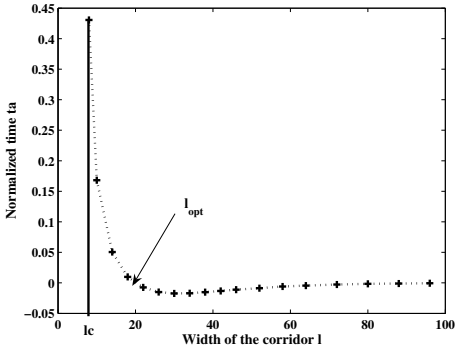

Figure 6. Time t_a versus the width of the corridor.

main (1), V_c is the wavefront velocity between two cells in the domain (1), V_o is the wavefront velocity between two

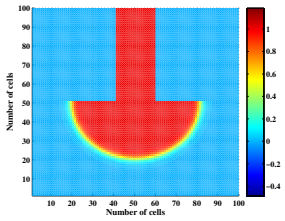

Figure 7. Propagation.

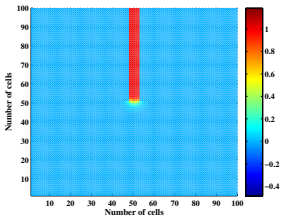

Figure 8. Blockage.

cells in the domain (2) and V_t is the wavefront velocity between one cell in the domain (1) and a second cell in the domain (2). As previously described, we initiate a planar wavefront in the corridor travelling towards the large area. Fig. 5 shows the different velocities of the wavefront when $\alpha = 0.4$ and $D = 0.5$, in function of l (expressed in cell number). The results indicate that the velocity of the circular wave in domain (2) depends on the width l of the strand. The width l of the strand changes the circular wave curvature. There exists a critical value l_c of l below which the wavefront fails to propagate through the subdomains interface, as shown in Fig. 8. When l is large enough, velocities are equal and the wavefront is no more influenced by the interface. Between these two cases, the symmetry breaking implies a time delay corresponding to the geometrical transformation of the wave from a planar to a non planar wavefront (see Fig. 7 for instance, where a circular wave appears just after the transition region). Let t_a be the necessary time needed to the wavefront to cross the interface so that

$$t_a = \frac{\frac{d_t}{V_t} - \frac{d_o}{V_o} - \frac{d_c}{V_c}}{\frac{d_o}{V_o} + \frac{d_c}{V_c}} \qquad (15)$$

with d_i, the distance between the different parts of the medium for which the velocity is V_i (i=$\{$t,o,c$\}$). Fig. 6 shows that this overall delay can be either positive or negative depending on the value of l. Note that delays may imply reentrant arrhythmias due to a lack of synchronicity between wavefront coming from different pathways. Our results indicate that, besides the case of large corridors, there exists an optimum width l_{opt} around which overall delays are negligible (see Fig. 6).Therefore, there is a possible relationship between length and width of corridors preventing dramatic changes of cardiac activity.

3. Discussion and conclusions

In this study, an analytical solution of travelling front in the case of the planar propagation has been determined. The criterion for the initiation of the circular waves has been investigated, based on the existence of standing waves. We showed that the existence of the standing wave prevents the propagation. Again, this breakdown depends not only on the nonlinearity threshold and on the diffusion coefficient but also on the geometrical morphology of the cardiac syncytium and on the form of the excitation wavefront. We suggest that this work could be applied to avoid the reentry phenomena. In other words, our results could modify the strategies used during arrhythmia ablation procedures. Indeed, precise radiofrequency applications inside scar tissues could improve conduction velocity in other areas and prevent reentries [15]. It would correspond to fix the optimized width so that the delay becomes negligible, which would assures synchronicity between waves coming from different pathways.

References

[1] Myerburg RJ, Interian A, Mitrami RM, Kessler KM, Castellanos A. Frequency of sudden cardiac death and profiles of risk. Am. J. Cardiology 1997;80:10F-19F.

[2] Saffitz JE. The pathology of sudden cardiac death in patients with ischemic heart disease-arrhythmology for anatomic pathologists. Cardiovascular Pathology 2005;14:195-203.

[3] Rohr S, Kucera JP, Kleber AG. Form and function: impulse propagation in designer cultures of cardiomyocytes. News Physiol. Sci.1997;12.

[4] Wang Y, Rudy Y. Action potential propagation in inhomogneous cardiac tissue: safety factor consideration and ionic mechanism. Am. J. Physiol. 2000;278:H1019.

[5] Fast VG, Kleber AG. Role of wavefront curvature in propagation of cardiac impulse. Cardiovascular Research 1997;33:258-271.

[6] Fast VG, Kleber AG. Cardiac tissue geometry as a determinant of unidirectional conduction block: assessment of microscopic excitation spread by optical mapping in patterned cell cultures and in a computer model. Cardiovascular Research 1995;29:697-707.

[7] Fast VG, Kleber AG. Block of impulse propagation at an abrupt tissue expansion: evaluation of the critical strand diameter in 2− and 3− dimensional computer models. Cardiovascular Research 1995;30:449-459.

[8] Kleber AG, Rudy Y. Basic mechanisms of cardiac impulse propagation and associated arrhythmias. Am. Physiol. Rev. 2004;84:431-488.

[9] Noble D. A modification of the Hodgkin-Huxley equation applicable to Purkinge fibre action and pacemaker potentials. J. Physiol 1962;160:317-352.

[10] Murray JD. Mathematical Biology. Springer Verlag, Berlin 1989.

[11] Keener J, Sneyd J. Mathematical Physiology. IAM, Springer-Verlag, Berlin 1998.

[12] Scott A. Nonlinear Science: Emergence and Dynamics of Coherent Structures. Oxford Univ. Press 1998.

[13] Nagumo J, Arimoto S, Yoshizawa S. An active impulse transmission line simulating nerve axon. Proc. IRE 1962;50:2061-2070.

[14] Zemskov EP, Zykov VS, Kassner K, Müller SC. Stability of travelling fronts in a piecewise-linear reaction-diffusion system. Nonlinearity 2000;13:2063-2076.

[15] Chillou C, Lacroix D, Klug D, Magnien-Poull I, Marquie C, Messier M, Andronache M, Kouakam C, Sadoul N, Chen J, Aliot E, Kacet S. Isthmus characteristics of reentrant ventricular tachycardia after myocardial infarction. Circulation 2002;105(6):726-31.

Address for correspondence:

Stéphane Binczak,
stbinc@u-bourgogne.fr
Laboratoire LE2I UMR CNRS 5158, 21078 Dijon, France.